

Cite this: *Dalton Trans.*, 2018, **47**,
1151

Electronic versus steric effects of pyridinophane ligands on Pd(III) complexes†

Fengzhi Tang,^{‡a} Sungho V. Park,^{‡a} Nigam P. Rath^b and Liviu M. Mirica^{ID} ^{*,a}

Several new Pd^{II} and Pd^{III} complexes supported by electronically and sterically tuned tetradentate pyridinophane ligands ^{Me}N4^{OMe}, ^{Me}N4, and ^{tBu}N4 were isolated and fully characterized (^{Me}N4^{OMe}: *N,N*-dimethyl-2,11-diaza[3,3](2,6)-*para*-methoxypyridinophane; ^{Me}N4: *N,N*-dimethyl-2,11-diaza[3,3](2,6)pyridinophane; ^{tBu}N4: *N,N*-di-*tert*-butyl-2,11-diaza[3,3](2,6)pyridinophane). Cyclic voltammetry studies, UV-vis and EPR spectroscopy, and X-ray crystallography were employed to reveal that the steric properties of the *N*-substituents of the ^RN4 ligands have a pronounced effect on the electronic properties of the corresponding Pd^{III} complexes, while the electronic tuning of the ligand pyridyl groups has a surprisingly minimal effect. An explanation for these observations was provided by DFT and TD-DFT calculations which suggest that the electronic properties of the Pd^{III} complexes are mainly dictated by their frontier molecular orbitals that have major atomic contributions from the Pd center (mainly the Pd *d*_{z²} atomic orbital) and the axial N atom donors.

Received 20th November 2017,
Accepted 11th December 2017

DOI: 10.1039/c7dt04366j

rsc.li/dalton

Introduction

Ligand modification *via* electronic and steric tuning has been broadly employed to understand the fundamentals of ligand design in organometallic chemistry and catalysis.^{1–4} The analysis of such steric and electronic effects can provide important insights into the development of novel catalytic systems with high reactivity and regio- and enantioselectivities.^{5–10} In the context of Pd catalysis, it has been shown recently that high-valent Pd^{III} and Pd^{IV} species are active intermediates in several stoichiometric and catalytic C–C and C–heteroatom bond transformations.^{11–18} Given our interest in Pd^{III} chemistry,^{19–27} probing the ligand effects onto the properties of the corresponding Pd^{III} complexes should provide insights toward the understanding of Pd^{III} reactivity and the development of catalysts involving Pd^{III} species.

In 2010, we have reported that a tetradentate ligand *N,N*-di-*tert*-butyl-2,11-diaza[3,3](2,6)pyridinophane (^{tBu}N4) can stabilize the paramagnetic Pd^{III} complexes that show unique properties due to the *d*⁷ electronic structure of the Pd center, as shown through various characterization methods such as

cyclic voltammetry (CV), UV-Vis and EPR spectroscopy, and X-ray crystallography.¹⁹ By decreasing the steric bulk of the *N*-substituents, the ligands ^{Me}N4 and ^{iPr}N4 were found to dramatically influence the properties of the corresponding Pd^{III} complexes such as their redox potentials, UV-vis absorptions, and EPR parameters. The X-ray structures of these isolated Pd^{III} complexes also reveal shorter Pd–N_{axial} bond distances (^{tBu}N4 > ^{iPr}N4 > ^{Me}N4) due to reduced steric interactions between the equatorial ligands and the *N*-substituents.^{18,26} Continuing the study of such uncommon mononuclear Pd^{III} complexes,^{18,25} we report herein the synthesis and characterization of Pd^{II} and Pd^{III} complexes supported by the ^{Me}N4^{OMe} ligand (*N,N*-dimethyl-2,11-diaza[3,3](2,6)-*p*-methoxypyridinophane) and the systematical comparison of their spectroscopic and structural properties with those of the analogous complexes supported by ^{Me}N4 and ^{tBu}N4 ligands, along with supporting DFT calculations.

Results and discussion

Synthesis of the ^{Me}N4^{OMe} ligand and the Pd complexes

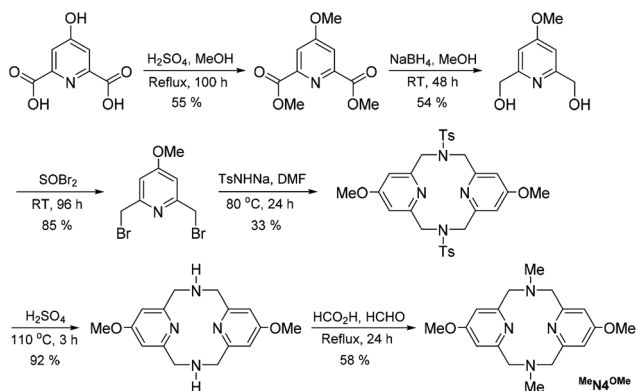
Our previous studies showed that the *N*-substituents of the ^RN4 ligand have a dramatic effect on the stability and reactivity of the corresponding Pd^{III} and Pd^{IV} complexes.¹⁸ In addition to this strong steric effect, the manipulation of the electronic properties of ^RN4 ligands was also considered to further tune the properties of high-valent Pd complexes. Thus, we sought to employ an electron-rich ^{Me}N4^{OMe} ligand containing an electron-donating methoxy group at the *para* position of the

^aDepartment of Chemistry, Washington University, One Brookings Drive, St Louis, Missouri 63130-4899, USA. E-mail: mirica@wustl.edu

^bDepartment of Chemistry and Biochemistry, University of Missouri-St Louis, One University Boulevard, St Louis, Missouri 63121-4400, USA

† Electronic supplementary information (ESI) available. CCDC 1583174–1583176. For ESI and crystallographic data in CIF or other electronic format see DOI: 10.1039/c7dt04366j

‡ These authors contributed equally to this work.



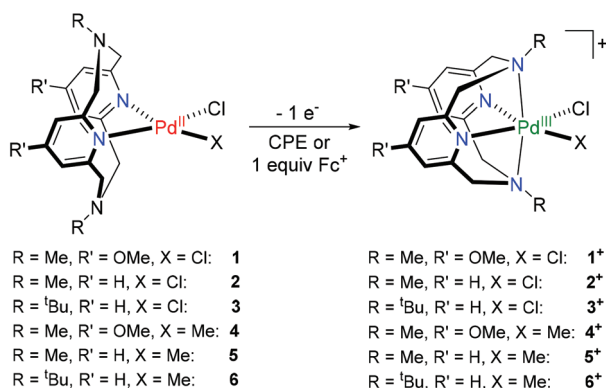
Scheme 1 Synthesis of the $^{\text{Me}}\text{N}_4^{\text{OMe}}$ ligand.

pyridyl groups. The synthesis of $^{\text{Me}}\text{N}_4^{\text{OMe}}$ employed chelidamic acid as the starting material and followed a slightly modified synthetic route to afford the target ligand $^{\text{Me}}\text{N}_4^{\text{OMe}}$ (Scheme 1).^{28,29}

The dichloride and methyl chloride ($^{\text{R}}\text{N}_4$) Pd^{II} complexes 1–6 were prepared by mixing the corresponding $^{\text{R}}\text{N}_4$ ligand with the Pd^{II} precursors (COD) PdCl_2 or (COD) PdMeCl in CH_2Cl_2 or Et_2O , respectively. While the ($^{\text{tBu}}\text{N}_4$) Pd^{II} complexes 3 and 6¹⁹ and ($^{\text{Me}}\text{N}_4$) Pd^{II} complexes 2 and 5²⁶ have been reported previously, the ($^{\text{Me}}\text{N}_4^{\text{OMe}}$) Pd^{II} complexes 1 and 4 are reported herein for the first time. Given the accessible oxidation potentials for all of these complexes (see below), they can be oxidized easily by one electron using either controlled potential electrolysis (CPE) or chemical oxidation with 1 equiv. of ferrocenium hexafluorophosphate (Fc^+PF_6^-) to yield the corresponding Pd^{III} complexes (Scheme 2). These Pd^{III} complexes are stable at room temperature and X-ray quality crystals can be obtained by Et_2O diffusion into the solutions of the complexes in DCM or MeCN at $-20\text{ }^\circ\text{C}$.³⁰

Comparison of the electronic properties of the Pd^{II} and Pd^{III} complexes

Electrochemical studies of the Pd^{II} complexes. The CV characterization of the dichloride Pd^{II} complexes 1–3 reveals



Scheme 2 Synthesis of the Pd^{III} complexes.^{19,25,26}

that the ($^{\text{Me}}\text{N}_4^{\text{OMe}}$) $\text{Pd}^{\text{II}}\text{Cl}_2$ complex 1 exhibits an $E_{\text{pa}}^{\text{II/III}}$ oxidation potential that is only 20 mV lower than the $E_{\text{pa}}^{\text{II/III}}$ for the ($^{\text{Me}}\text{N}_4$) $\text{Pd}^{\text{II}}\text{Cl}_2$ complex 2, while the ($^{\text{tBu}}\text{N}_4$) $\text{Pd}^{\text{II}}\text{Cl}_2$ complex 3 has an $E_{\text{pa}}^{\text{II/III}}$ oxidation potential that is ~ 180 mV higher than that for 2. In addition, the $E_{1/2}\text{Pd}^{\text{III/IV}}$ values for 1 and 2 are within 20 mV of each other, while the $E_{1/2}\text{Pd}^{\text{III/IV}}$ value for 3 is ~ 300 mV higher than those for 1 and 2. A similar trend is observed for the $\text{Pd}^{\text{II}}\text{MeCl}$ complexes 4–6, where the $E_{\text{pa}}^{\text{II/III}}$ oxidation potential for the $^{\text{tBu}}\text{N}_4$ complex 6 is ~ 170 mV higher than those for complexes 4/5, while the $E_{1/2}\text{Pd}^{\text{III/IV}}$ value for the $^{\text{tBu}}\text{N}_4$ complex 6 is ~ 380 mV higher than those for complexes 4/5 (Fig. 1 and Table 1). Overall, these results suggest that increasing the electron-donating ability of the pyridyl groups has a minimal effect on the electrochemical properties of the corresponding Pd complexes, while the nature of the N -substituent has a more pronounced effect on these redox properties of Pd complexes, most likely by directly modulating the energy and atomic orbital (AO) contributions of the frontier molecular orbitals (FMOs) of these Pd complexes (see below).

UV-Vis absorption spectroscopy of the Pd^{III} complexes. The UV-Vis spectra of complexes 1⁺–6⁺ exhibit two strong absorption bands at 578–723 nm and 303–395 nm that are assigned as LMCT bands (Table 1), as reported previously.¹⁹ The steric manipulation of the N -substituents greatly influences the absorption properties of the Pd^{III} complexes, as the ($^{\text{tBu}}\text{N}_4$) $\text{Pd}^{\text{III}}\text{Cl}_2$ and $\text{Pd}^{\text{III}}\text{MeCl}$ complexes 3⁺ and 6⁺ show transitions that are red shifted by 100–150 nm vs. those for the analogous complexes 2⁺ and 5⁺ supported by the less bulky $^{\text{Me}}\text{N}_4$ ligand.²⁶ By comparison, the Pd complexes 1⁺ and 4⁺ of the more electron-rich $^{\text{Me}}\text{N}_4^{\text{OMe}}$ ligand exhibit UV-Vis spectra similar to those of analogous ($^{\text{Me}}\text{N}_4$)Pd complexes 2⁺ and 5⁺ (Fig. 2 and Table 1), suggesting that the MOs involved in the transitions of these Pd^{III} complexes have negligible contributions from the pyridine-based AOs.

EPR spectroscopy of the Pd^{III} complexes. The EPR spectra collected at 77 K for the Pd^{III} complexes reveal axial signals for the $\text{Pd}^{\text{III}}\text{Cl}_2$ complexes 1⁺–3⁺ and rhombic patterns for the $\text{Pd}^{\text{III}}\text{MeCl}$ complexes 4⁺–6⁺, yet all suggesting a Pd^{III} center with a d_{z^2} ground state (Fig. 3). The axial superhyperfine coupling constants of the Pd^{III} complexes supported by $^{\text{Me}}\text{N}_4^{\text{OMe}}$ and $^{\text{Me}}\text{N}_4$ ligands were identical (25.5 G for 1⁺ and 2⁺, 23.0 G for 4⁺ and 5⁺, Table 1), implying a similar extent of interaction

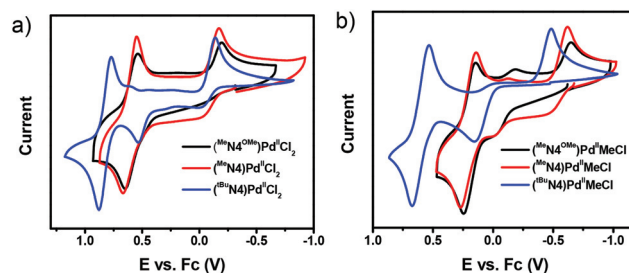


Fig. 1 Overlay of CV traces (0.1 M $\text{Bu}_4\text{NClO}_4/\text{DCM}$, 100 mV s^{-1} scan rate) for (a) $\text{Pd}^{\text{III}}\text{Cl}_2$ complexes 1⁺–3⁺ and (b) $\text{Pd}^{\text{III}}\text{MeCl}$ complexes 4⁺–6⁺.

Table 1 Spectroscopic and electrochemical properties of the Pd^{III} complexes

	$E_{pc}^{III/II}$, $E_{pa}^{II/III}$, $E_{1/2}^{III/IV}$ (ΔE_p) ^a , mV	UV-vis (MeCN) λ , nm (ϵ , M ⁻¹ cm ⁻¹)	EPR ^b g_x , g_y , g_z , (A_{2N} , G) ^c
1 ⁺	-195, -40, 595 (110)	583 (960), 365 (sh, 2260), 325 (sh, 3060)	2.129, 2.129, 2.004 (25.5)
2 ⁺	-175, -45, 610 (115)	578 (1420), 362 (2440)	2.126, 2.126, 2.004 (25.5)
3 ⁺ ^d	-18, 117/626 ^e , 918 (76)	716 (1820), 395 (2780)	2.152, 2.142, 2.000 (23.0)
4 ⁺	-650/-185 ^e , -50, 195 (100)	615 (560), 495 (380), 303 (4700)	2.219, 2.108, 2.016 (23.0)
5 ⁺ ^d	-620/-135 ^e , -480/-20 ^e , 205 (130)	606 (615), 475 (480), 316 (3550)	2.212, 2.101, 2.014 (23.0)
6 ⁺ ^d	-464, 134, 587 (63)	723 (1100), 545 (490), 368 (3300)	2.239, 2.134, 2.005 (19.5)

^a Redox potentials are reported vs. Fc/Fc⁺ in 0.1 M Bu₄NClO₄/MeCN or DCM, scan rate 100 mV s⁻¹; ΔE_p is the peak potential separation for the Pd^{III}/Pd^{IV} couple. ^b In 3 : 1 PrCN : MeCN glass, 77 K. ^c Superhyperfine coupling to the two axial N donors ($I = 1$). ^d The CV and UV-vis data for 3⁺, 5⁺, and 6⁺ are from ref. 25, 26, and 19, respectively. ^e The duplicate $E_{pa}^{III/II}$ and $E_{pc}^{II/III}$ values are likely due to two conformations present in solution (ref. 25).

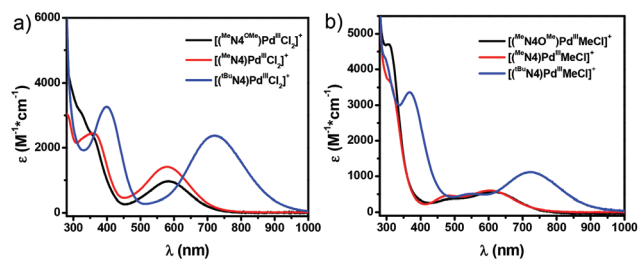


Fig. 2 Overlay of UV-Vis spectra in MeCN for (a) Pd^{III}Cl₂ complexes 1⁺–3⁺ and (b) Pd^{III}MeCl complexes 4⁺–6⁺.

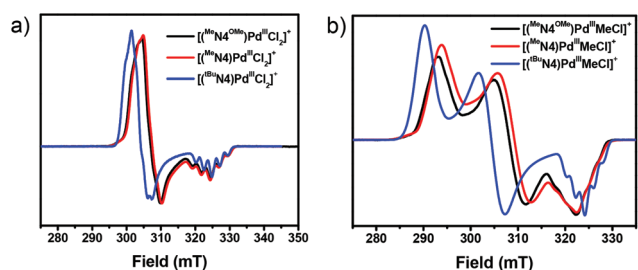


Fig. 3 Overlay of EPR spectra (frozen glasses in 1 : 3 MeCN : PrCN, 77 K) for (a) Pd^{III}Cl₂ complexes 1⁺–3⁺ and (b) Pd^{III}MeCl complexes 4⁺–6⁺.

between the Pd^{III} center and the axial N donors, despite the different electronic properties of the pyridyl groups for the two ligands. In contrast, the ^tBuN₄-supported Pd^{III} complexes 3⁺ and 6⁺ exhibit superhyperfine coupling constants that are ~3 G smaller than those of the other complexes, suggesting a weaker Pd^{III}-N_{axial} interaction. In addition, the ^{Me}N₄^{OMe} and ^{Me}N₄ Pd^{III} complexes showed smaller differences between g_x/g_y values and g_z values than those of the ^tBuN₄ supported analogues, which could be attributed to a more symmetric geometry around the Pd^{III} center (see below).

Structural comparison of the Pd^{III} complexes. All the single crystal X-ray characterizations of complexes [1⁺]ClO₄, [2⁺]ClO₄, and [4⁺]ClO₄ revealed Pd^{III} centers in a distorted octahedral geometry, similar to the other reported analogous Pd^{III} complexes [3⁺]ClO₄, [5⁺]ClO₄, and [6⁺]ClO₄ (Fig. 4–6 and Fig. S25, S26[†]).^{19,26} Surprisingly, all the metrical parameters of the Pd^{III} centers in the ^{Me}N₄^{OMe}-supported complexes 1⁺ and 4⁺ are

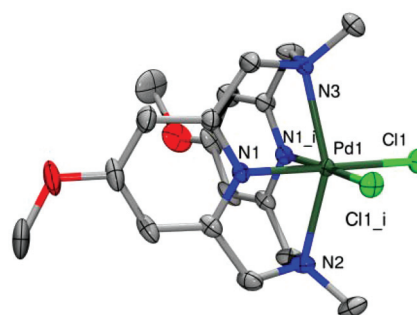


Fig. 4 ORTEP representation (50% probability ellipsoids) of 1⁺. Selected bond distances (Å) and angles (°): 1⁺: Pd1–N1 2.0009(19), Pd1–N1_i 2.0009(18), Pd1–N2 2.300(3), Pd1–N3 2.308(3), Pd1–Cl1 2.3018(6), Pd1–Cl1_i 2.3018(6), N1–Pd1–N1_i 82.67(11), N2–Pd1–N3 152.89(10).

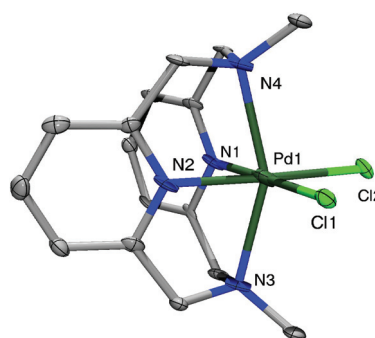


Fig. 5 ORTEP representation (60% probability ellipsoids) of 2⁺. Selected bond distances (Å) and angles (°): 2⁺: Pd1–N1 2.029(8), Pd1–N2 2.002(8), Pd1–N3 2.310(9), Pd1–N4 2.311(9), Pd1–Cl1 2.303(3), Pd1–Cl2 2.322(3), N1–Pd1–N2 82.3(3), N3–Pd1–N4 153.5(3).

almost identical to those of the ^{Me}N₄ Pd^{III} complexes, suggesting a minimal effect of the electron-donating *p*-methoxy group on the Pd^{III} center. However, the Pd–N_{ax} bond distances in the ^tBuN₄-supported Pd^{III} complexes 3⁺ and 6⁺ are ~0.1 Å longer than those in ^{Me}N₄ supported analogs – likely due to the increased steric clash between the *N*-substituents and equatorial CH₃ or Cl ligands.²⁶ In addition, this steric hindrance also leads to an overall distortion of complexes 3⁺ and 6⁺ such that the pyridyl is tilted in the opposite direction relative to the equatorial plane, in order to accommo-

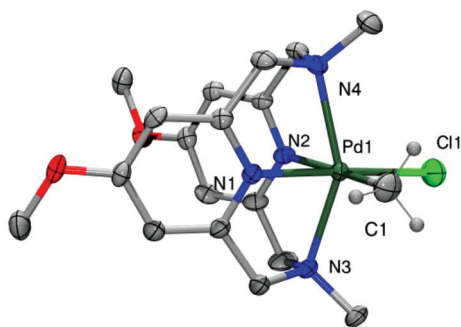


Fig. 6 ORTEP representation (50% probability ellipsoids) of 4^+ . Selected bond distances (Å) and angles ($^\circ$): 4^+ : Pd1–N1 2.055(3), Pd1–N2 2.130(3), Pd1–N3 2.297(3), Pd1–N4 2.340(3), Pd1–C1 2.040(4), Pd1–Cl1 2.3298 (11), N1–Pd1–N2 81.09(12), N3–Pd1–N4 149.19(11).

date the bulkier *t*-butyl *N*-substituents (see the space-filling models in Fig. S25 and S26[†]).³⁰ Overall, these structural characteristics of the Pd^{III} complexes further suggest that the steric modulation of the *N*-substituent has a more pronounced effect than the electronic donation ability of the pyridyl groups.

Computational studies. It is known that the electronic and chemical properties of a metal complex are closely related to its frontier molecular orbitals (FMOs).³¹ Therefore, DFT studies were employed in order to investigate the ground state electronic structures of our family of Pd^{III} complexes, with special emphasis on the FMO energies and the atomic contribution to the FMOs α -HOMOs and β -LUMOs. In addition, TD-DFT calculations were used to calculate the absorption spectra assigned to the observed transitions for these Pd^{III} complexes.

For all Pd^{III} complexes $1^+–6^+$, the electron densities for both the α -HOMOs and β -LUMOs are localized mainly along the axial direction, with $\sim 30\%$ contribution from the Pd center (almost exclusively the d_{z^2} atomic orbital) and $\sim 40\%$ contribution from the N_{axial} atoms (Fig. 7 and Tables S1–S8[†]).³⁰ In contrast, the contributions from the equatorial atom donors are minimal ($<6\%$). This further supports the experimental observation that altering the *N*-substituents of the axial N donor atoms has a more prominent effect than modifying the equatorial pyridyl groups. Interestingly, the atomic contributions to the α -HOMOs and β -LUMOs for all complexes $1^+–6^+$ are almost identical for the $\text{MeN}_4\text{Pd}^{\text{III}}$ and $\text{MeN}_4^{\text{OMe}}\text{Pd}^{\text{III}}$ complexes, revealing that the electronic tuning of the pyridyl groups has a negligible effect. This also provides an explanation why the electronic properties of the two series of Pd^{III} complexes are similar. In contrast, the ${}^t\text{BuN}_4\text{Pd}^{\text{III}}$ complexes 3^+ and 6^+ exhibit less covalent metal–axial ligand interactions, as suggested by the slightly smaller contributions from the Pd centers and N_{axial} ligands to the FMOs (Fig. 7 and Tables S1–S8[†]),³⁰ which is likely due to the steric clash between the bulky *t*-Bu *N*-substituents and the equatorial ligands that leads to a distortion of the Pd^{III} complex geometry (Fig. S25[†]).³⁰ This also correlates with the metrical parameters obtained from the X-ray characterization of these complexes showing that

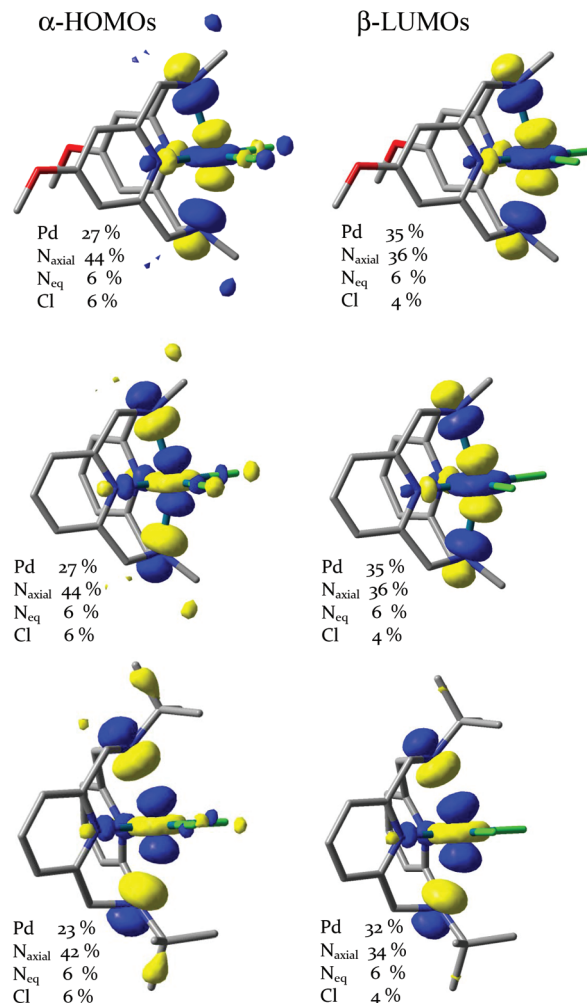


Fig. 7 Comparison of the DFT-calculated α -HOMOs, β -LUMOs, and their atomic contributions for Pd^{III}Cl₂ complexes 1^+ (top), 2^+ (middle), and 3^+ (bottom).

Pd– N_{axial} bond distances for the ${}^t\text{BuN}_4\text{Pd}^{\text{III}}$ complexes are ~ 0.1 Å longer than those of the corresponding MeN_4 and $\text{MeN}_4^{\text{OMe}}$ complexes (Table 2). The less covalent Pd– N_{axial} interactions in the ${}^t\text{BuN}_4\text{Pd}^{\text{III}}$ complexes can also explain their smaller super-hyperfine coupling constants observed in the EPR spectra (Table 1), as well as the red shift observed in the UV-vis spectra of complexes 3^+ and 6^+ (Fig. 2). The TD-DFT calculated UV-Vis spectra and electronic transitions for complexes $1^+–6^+$ match well with the experimental spectra (Fig. S27 and S38[†]),³⁰ and the absorptions at 578–723 nm are assigned to β -HOMO to β -LUMO LMCT transitions. The DFT calculations indeed show that the HOMO–LUMO gaps for the MeN_4 and $\text{MeN}_4^{\text{OMe}}$ Pd^{III} complexes are similar, while the HOMO–LUMO gaps for the ${}^t\text{BuN}_4\text{Pd}^{\text{III}}$ analogs are ~ 0.7 eV smaller (Fig. 8), which leads to the 100–150 nm red shift for the corresponding absorption bands. Finally, the HOMOs of complexes 3^+ and 6^+ are slightly higher in energy than those of the other complexes, which supports their observed higher Pd^{III/IV} (and Pd^{II/III}) redox potentials (Fig. 1 and Table 1).

Table 2 Selected bond distances and angles for the Pd^{III} complexes 1⁺–6⁺

	Pd–N _{ax}	Pd–N _{eq}	Pd–Cl	Pd–C	N _{ax} –Pd–N _{ax}	N _{eq} –Pd–N _{eq}
1 ⁺	2.304(3)	2.0009(19)	2.3018(6)	NA ^a	152.89(10) ^o	82.67(11) ^o
2 ⁺	2.310(9)	2.016(8)	2.312(3)	NA ^a	153.5(3) ^o	82.3(3) ^o
3 ⁺ ^b	2.417(2)	2.003(2)	2.3160(7)	NA ^a	145.07(7) ^o	88.06(9) ^o
4 ⁺	2.318(3)	2.092(3)	2.3298(11)	2.040(4)	149.19(11) ^o	81.09(12) ^o
5 ⁺ ^b	2.320(3)	2.085(2)	2.344(3)	2.021(11)	149.12(11) ^o	81.44(12) ^o
6 ⁺ ^b	2.4268(16)	2.0585(16)	2.3403(5)	2.0921(18)	142.37(5) ^o	86.61(6) ^o

^a Not applicable. ^b Bond distances and angles for 3⁺, 5⁺, and 6⁺ are from ref. 25, 26, and 19, respectively.

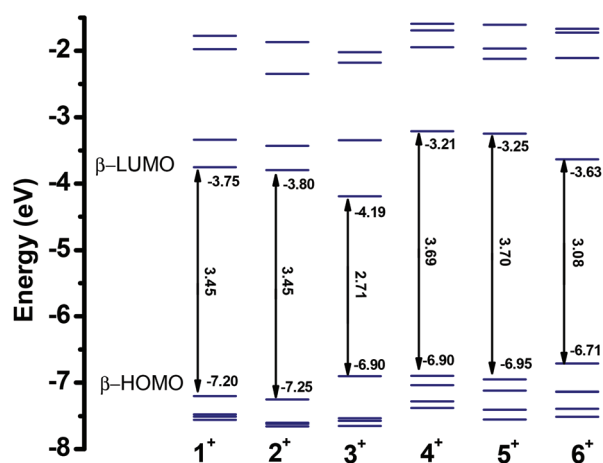


Fig. 8 Pictorial representation of the FMO energy levels (β AOs) for complexes 1⁺–6⁺.

Conclusion

In summary, we report herein the synthesis of the electronically tuned pyridinophane ligand ^{Me}N4^{OMe} and the corresponding Pd^{II} and Pd^{III} complexes, as well as a systematic comparison of the properties of the Pd^{III}Cl₂ and Pd^{III}MeCl complexes supported by the ^{Me}N4^{OMe}, ^{Me}N4, and ^{tBu}N4 ligands. Remarkably, the ^{Me}N4^{OMe} and ^{Me}N4 Pd^{III} complexes have almost identical spectroscopic and structural properties, as observed by cyclic voltammetry studies, UV-vis and EPR spectroscopy, and X-ray crystallography. In contrast, the steric properties of the *N*-substituents of the ^RN4 ligands have a pronounced effect on the electronic and structural properties of the corresponding Pd complexes, as observed for the ^{tBu}N4-supported Pd^{III} complexes. To support these experimental observations, DFT and TD-DFT calculations were employed to reveal that the electronic properties of the Pd^{III} complexes are mainly dictated by their frontier molecular orbitals that have major atomic contributions from the Pd center (mainly the Pd d_{z²} atomic orbital) and the N_{axial} atom donors. Overall, these results suggest that the properties as well as the nature^{23,24} of the axial atom donors have a pronounced effect on the stability and ultimately reactivity of the corresponding Pd^{III} centers, and d₇ ions in general, and further expansion of the ligand systems employed should be mainly aimed at modifying the coordination properties and identity of the axial atom donors.

Experimental section

General experimental details

All operations were performed under a nitrogen atmosphere using standard Schlenk and glove box techniques if not indicated otherwise. All reagents for which the syntheses are not given were purchased from Fisher Scientific, Sigma-Aldrich, Acros, STREM, or Pressure Chemical and were used as received without further purification. Solvents were purified prior to use by passing them through a column of activated alumina using an MBRAUN SPS. The synthesis and characterization of complexes (^{Me}N4)Pd^{II}Cl₂, [(^{Me}N4)Pd^{II}MeCl]⁺, and [(^{Me}N4)Pd^{III}MeCl]⁺ have been reported previously.²⁷ NMR spectra were obtained on a Varian Mercury-300 spectrometer (300.121 MHz) or a Varian Unity Inova-600 spectrometer (599.746 MHz). Chemical shifts are reported in parts per million (ppm) with residual solvent resonance peaks as internal references.⁴ Abbreviations for the multiplicity of NMR signals are singlet (s), doublet (d), triplet (t), quartet (q), septet (sep), multiplet (m), and broad resonance (br). UV-vis spectra were recorded on a Varian Cary 50 Bio spectrophotometer and are reported as λ_{max} , nm (ϵ , M⁻¹ cm⁻¹). EPR spectra were recorded on a JEOL JES-FA X-band (9.2 GHz) EPR spectrometer in 3:1 PrCN:MeCN at 77 K or 293 K. Solution magnetic susceptibility measurements for the Pd^{III} complexes were obtained at 293 K with the Evans method,³² including the corresponding diamagnetic corrections.³³ ESI-MS experiments were performed using a linear quadrupole ion trap Fourier transform ion cyclotron resonance mass spectrometer (LTQ-FTMS, Thermo, San Jose, CA) or a Bruker Maxis Q-TOF mass spectrometer with an electrospray ionization source. ESI mass-spectrometry was provided by the Washington University Mass Spectrometry Resource. Elemental analyses were carried out by the Columbia Analytical Services Tucson Laboratory and Intertek Pharmaceutical Services.

Electrochemical studies

Cyclic voltammetry (CV) studies were performed with a BASI EC Epsilon electrochemical workstation or CHI Electrochemical Analyzer 660D. Electrochemical grade Bu₄NClO₄ from Fluka was used as the supporting electrolyte. The electrochemical measurements were performed under a blanket of nitrogen, and the analyzed solutions were deaerated by purging with nitrogen. A glassy carbon disk electrode (GCE)

was used as the working electrode, and a Pt wire as the auxiliary electrode. The non-aqueous Ag-wire reference electrode assembly was filled with 0.01 M AgNO₃/0.1 M Bu₄NClO₄/MeCN solution. The reference electrodes were calibrated against ferrocene for each CV measurement.

Bulk electrolysis oxidations were performed in a two-compartment bulk electrolysis cell (BASi) separated by a fine-frit glass junction at room temperature. A reticulated vitreous carbon working electrode was used in the anodic compartment equipped with a magnetic stirring bar. A Pt gauze (25 mm × 10 mm) was used as the auxiliary electrode in the cathodic compartment. A non-aqueous Ag/0.01 M AgNO₃ electrode was used as the reference electrode. Prior to electrolysis, a CV of the Pd^{II} precursor was performed in the same setup. The potential of electrolysis was set to be 100 mV–200 mV, more positive than the corresponding oxidation peak potential observed in the CV scan. Electrochemical grade Bu₄NClO₄ from Fluka was used as the supporting electrolyte.

Synthetic procedures

4-Methoxypyridine-2,6-dicarboxylic acid dimethyl ester.²⁸

Chelidamic acid monohydrate (1.31 g) was refluxed in ~300 mL dry methanol in the presence of 6 mL concentrated sulfuric acid for 4 days. After cooling down to RT, sodium carbonate (1 equiv. relative to the amount of sulfuric acid) was added and the solvent was removed. The residue was dissolved in saturated aqueous sodium bicarbonate solution and then extracted with dichloromethane (DCM). The organic layer was dried over sodium sulfate and filtered, the solvent was removed and the white solid was dried *in vacuo*. Yield: 0.81 g (55%). ¹H NMR (300 MHz, CDCl₃), δ: 7.82 (s, 2H, arom-H), 4.01 (s, 6H, –COOCH₃), 3.98 (s, 3H, *p*-OCH₃).

4-Methoxy-2,6-bis(hydroxymethyl)pyridine. To 2.22 g of 4-methoxypyridine-2,6-dicarboxylic acid dimethyl ester in 50 mL methanol, sodium borohydride (5 equiv., 1.86 g) was slowly added. As the mixture refluxed, the color changed from colorless to yellow, and then to white. The resulting solution was stirred at room temperature for 2 days. The solvent was then removed under reduced pressure and the residue was dissolved in 30 mL of saturated NaHCO₃ solution. The solution was extracted with DCM, and the organic and aqueous layers were dried separately. The aqueous layer residue was extracted with 100 mL chloroform using a Soxhlet extractor for 2 days at 80 °C. Yield: 0.90 g (54%). ¹H NMR (300 MHz, CDCl₃), δ: 6.71 (s, 2H, arom-H), 4.71 (s, 4H, –CH₂–), 3.86 (s, 3H, *p*-OCH₃).

4-Methoxy-2,6-bis(bromomethyl)pyridine. 4-Methoxy-2,6-bis(hydroxymethyl)pyridine (2.97 g) was suspended in 125 mL dry DCM. A mixture of thionyl bromide (5 mL, 3.5 equiv.) in 35 mL DCM was added dropwise at 0 °C. The mixture was stirred for 4 days in the dark, and then it was poured into 100 mL of ice-cold water. The aqueous layer was neutralized to pH 8 with 3 M NaOH on an ice bath. The organic layer was separated, washed with 100 mL 1 M NaOH and then with 100 mL water. The DCM layer was then dried over sodium sulfate, filtered and concentrated to dryness. Yield: 4.41 g

(85%). ¹H NMR (300 MHz, CDCl₃), δ: 6.89 (s, 2H, arom-H), 4.48 (s, 4H, –CH₂–), 3.88 (s, 3H, *p*-OCH₃).

Methoxy *N,N'*-ditosyl-2,11-diaza[3.3](2,6)pyridinophane. 4-Methoxy-2,6-bis(bromomethyl)pyridine (4.41 g) in 40 mL anhydrous DMF was added dropwise to 2.884 g TsNHNHNa in 300 mL anhydrous DMF at 80 °C. After the addition was complete, stirring was continued at 80 °C for another hour. Another 2.884 g of TsNHNHNa was added all at once and heated at 80 °C overnight. After 24 h, the reaction mixture was cooled down to room temperature and the solvent was removed under reduced pressure. The brown residue was stirred with 150 mL MeOH for 10 minutes. The resulting suspension was filtered, then washed with water and a small amount of methanol. The light yellow solid was dried *in vacuo*. Yield: 0.75 g (33%). ¹H NMR (300 MHz, CDCl₃), δ: 7.68 (d, *J* = 8 Hz, 4H, tosyl-arom-H), 7.35 (d, *J* = 8 Hz, 4H, tosyl-arom-H), 6.94 (s, 4H, pyr-arom-H), 4.92 (s, 8H, –CH₂–), 4.00 (s, 6H, *p*-OCH₃), 2.42 (s, 6H, tosyl-CH₃).

Methoxy 2,11-diaza[3.3](2,6)pyridinophane (^HN₄^{OMe}). To 1.75 g of *p*-methoxy *N,N'*-ditosyl-2,11-diaza[3.3](2,6)pyridinophane, 13.7 mL of 90% H₂SO₄ was added and the solution was stirred at 110 °C for 3 hours. After cooling down to room temperature, the solution was diluted with 65 mL water and treated with 3 M NaOH to adjust the pH to 12–13. The resulting solution was extracted with DCM 3 times, dried over Na₂SO₄, and dried under vacuum. Yield: 0.77 g (92%). ¹H NMR (300 MHz, CDCl₃), δ: 6.06 (s, 4H, arom-H), 3.86 (s, 8H, –CH₂–), 3.66 (s, 6H, *p*-OCH₃).

Methoxy *N,N'*-dimethyl-2,11-diaza[3.3](2,6)pyridinophane (^{Me}N₄^{OMe}). An Eschweiler–Clarke methylation was conducted by dissolving 0.77 g of ^HN₄^{OMe} in 114 mL HCOOH and 25 mL 37% CH₂O. The mixture was refluxed under nitrogen for 1 day. After cooling, the reaction mixture was treated with 13.6 mL 37% HCl and the solvent was removed under reduced pressure. The residue was diluted with 10 mL H₂O and basified with 1 M NaOH to pH 13. The mixture was extracted with DCM 3 times, and the organic layer was dried over Na₂SO₄, filtered, and dried under vacuum. The white product was further purified by extraction into hexane and removal of the solvent. Yield: 580 mg (58%). ¹H NMR (300 MHz, CD₃CN), δ: 6.35 (s, 4H, arom-H), 3.64 (s, 8H, –CH₂–), 3.63 (s, 6H, *p*-OCH₃), 2.63 (s, 6H, N-CH₃). ¹³C NMR (300 MHz, CDCl₃), δ: 165.39 (py-*C*_{ortho}), 159.04 (py-*C*_{meta}), 109.16 (py-*C*_{para}), 65.94 (–CH₂–), 54.94 (*p*-OCH₃), 49.06 (*N*-methyl-C).

(^{Me}N₄^{OMe})Pd^{II}Cl₂, **1.** ^{Me}N₄^{OMe} (47.2 mg, 0.144 mmol) and (COD)Pd^{II}Cl₂ (41.0 mg, 0.144 mmol) were dissolved in 3 mL of DCM, separately. The ligand solution was added dropwise to the precursor solution under stirring. After the addition was complete, the reaction mixture was stirred for an additional 24 hours in the dark. The clear, dark yellow solution eventually turned cloudy. The solvent was removed and the residue was dissolved in a minimum (2 mL) of DCM. This yellow mixture was filtered, washed with ether and pentane, and dried *in vacuo*. Yield: yellow powder, 62.9 mg, 86%. ¹H NMR (300 MHz, CDCl₃): 6.65 (d, *J* = 15 Hz, 4H, –CH₂–), 6.61 (s, 4H, arom-H), 4.25 (d, *J* = 15 Hz, 4H, –CH₂–), 3.81 (s, 6H, *p*-OCH₃), 2.33 (s, 6H, N-CH₃). ESI-MS of (^{Me}N₄^{OMe})Pd^{II}Cl₂ in MeCN, *m/z* 469.0643; calculated

for $[M - Cl]^+$, $C_{18}H_{24}ClN_4O_2Pd$, 469.0643. Anal. found: C, 41.26; H, 4.46; N, 10.07; calcd for $(^{Me}N_4^{OMe})Pd^{III}Cl_2 \cdot \frac{1}{2}CH_2Cl_2$ ($C_{18}H_{24}Cl_2N_4O_2Pd$) $\cdot \frac{1}{2}CH_2Cl_2$: C, 40.53; H, 4.60; N, 10.22.

$(^{Me}N_4^{OMe})Pd^{III}MeCl$, **4**. Under a nitrogen atmosphere, the $^{Me}N_4^{OMe}$ ligand (44.3 mg, 0.135 mmol) and (COD) $Pd^{II}MeCl$ precursor (35.5 mg, 0.135 mmol) were loaded in a round bottom flask. Anhydrous ethyl ether (13.7 mL) was added, and a light yellow suspension immediately formed. This suspension was stirred for 48 hours in the dark. The pale yellow precipitate was filtered, washed with ether and pentane and dried *in vacuo*. Yield: 45.5 mg, 70%. 1H NMR (300 MHz, $CDCl_3$): 6.75 (s, 2H, arom-H), 6.75 (s, 2H, arom-H), 6.07 (d, $J = 12$ Hz, 2H, $-CH_2-$), 5.89 (d, $J = 12$ Hz, 2H, $-CH_2-$), 4.21 (d, $J = 12$ Hz, 2H, $-CH_2-$), 4.08 (d, $J = 12$ Hz, 2H, $-CH_2-$), 3.77 (s, 6H, $p-OCH_3$), 2.31 (s, 6H, N- CH_3), 0.41 (s, 3H, Pd- CH_3). ESI-MS of $(^{Me}N_4^{OMe})Pd^{II}MeCl$ in MeCN, m/z 449.1105; calculated for $[M - Cl]^+$, $C_{19}H_{27}N_4O_2Pd$, 449.1169. Anal. found: C, 47.52; H, 5.66; N, 11.29; calcd for $(^{Me}N_4^{OMe})Pd^{II}MeCl$ ($C_{19}H_{27}ClN_4O_2Pd$): C, 47.02; H, 5.61; N, 11.54.

$[(^{Me}N_4^{OMe})Pd^{III}Cl_2]ClO_4$, $[1^+]ClO_4$. The controlled potential electrolysis of $(^{Me}N_4^{OMe})Pd^{II}Cl_2$ (80 mg, 0.166 mmol) was performed in 12 mL of 0.03 M $Bu_4NClO_4/MeCN$ inside the working compartment of the electrolysis cell, while 12 mL 0.03 M $Bu_4NClO_4/MeCN$ solution was inside the auxiliary compartment. The electrolysis potential was set as 260 mV vs. Ag/0.01 M $AgNO_3$ based on the CV measurement in the same electrolysis cell. The color of the solution turned dark purple quickly during the electrochemical oxidation. The electrolysis was stopped after the charge corresponding to a one-electron oxidation has passed through the cell. The remaining dark purple solution was filtered and then diethyl ether was diffused at -20 °C for a few days to afford dark blue crystals suitable for X-ray crystallography. The crystals were filtered, washed with ether and pentane and dried *in vacuo*. Yield: 40 mg, 40%. UV-vis (MeCN), λ , nm (ϵ , $M^{-1} cm^{-1}$): 583 (960), 365 (2260), 325 (3060). ESI-MS $[(^{Me}N_4^{OMe})Pd^{III}Cl_2]^+$ in MeCN, m/z 484.0851; calcd for $[(^{Me}N_4^{OMe})Pd^{III}Cl_2]^+$, 484.0857. Anal. found: C, 37.46; H, 4.43; N, 10.51; calcd for $[C_{18}H_{24}Cl_3N_4O_6Pd \cdot CH_3CN]$: C, 37.17; H, 4.21; N, 10.84. $\mu_{eff}(CD_3CN) = 1.86\mu_B$.

$[(^{Me}N_4)Pd^{III}Cl_2](ClO_4)_2$, $[2^+]ClO_4$. The controlled potential electrolysis of $(^{Me}N_4)Pd^{II}Cl_2$ (74.1 mg, 0.166 mmol) was performed in 12 mL 0.03 M $Bu_4NClO_4/MeCN$ inside the working compartment of the electrolysis cell, while 12 mL 0.03 M $Bu_4NClO_4/MeCN$ solution was inside the auxiliary compartment. The electrolysis potential was set as 470 mV vs. Ag/0.01 M $AgNO_3$ based on the CV measurement in the same electrolysis cell. The color of the solution turned dark purple quickly during the electrochemical oxidation process. The electrolysis was stopped when the electrolysis current decreased to <5 μA . The dark purple solution in the working compartment was filtered and the filtrate was set for ether diffusion at -20 °C, to afford dark purple needle crystals suitable for X-ray crystallography after a few days. The crystals were filtered, washed with ether and pentane and dried *in vacuo*. Yield: 41.4 mg, 45%. UV-vis (CH_3CN), λ , nm (ϵ , $M^{-1} cm^{-1}$): 578 (1420), 362 (2440). ESI-MS of solution of $[(^{Me}N_4)Pd^{III}Cl_2](ClO_4)_2$ in MeCN, m/z

444.0107; calculated for $[(^{Me}N_4)Pd^{III}Cl_2]^+$, $C_{16}H_{20}Cl_2N_4Pd$, 444.0100. Anal. found: C, 36.87; H, 4.14; N, 11.54; calcd for $[(^{Me}N_4)Pd^{III}Cl_2](ClO_4) \cdot MeCN$ ($C_{18}H_{23}Cl_3N_4O_4Pd$): C, 36.88; H, 3.95; N, 11.95. $\mu_{eff}(CD_3CN) = 1.91\mu_B$.

$[(^{Me}N_4^{OMe})Pd^{III}MeCl]ClO_4$, $[4^+]ClO_4$. Ferrocenium hexafluorophosphate (18.1 mg, 0.055 mmol) and **4** (26.0 mg, 0.054 mmol) were combined in 5 mL MeCN and stirred for 30 minutes. The resulting solution was washed with pentane and concentrated with a rotary evaporator. The resulting dark purple residue was dissolved in a minimum amount of MeCN, and a concentrated solution of $LiClO_4$ was added and ether was then diffused at -20 °C. Yield: 6.3 mg, 60%. UV-vis (MeCN), λ , nm (ϵ , $M^{-1} cm^{-1}$): 615 (560), 495 (380), 303 (4700). ESI-MS $[(^{Me}N_4^{OMe})Pd^{III}MeCl]^+$ in MeCN, m/z 504.0293; calcd for $[(^{Me}N_4^{OMe})Pd^{III}MeCl]^+$, 504.0311. Anal. found: C, 40.71; H, 4.82; N, 10.84; calcd for $[C_{19}H_{27}Cl_2N_4O_6Pd \cdot CH_3CN]$: C, 40.30; H, 4.83; N, 11.19. $\mu_{eff}(CD_3CN) = 1.88\mu_B$.

X-ray crystallography

X-ray quality crystals of $[1^+]ClO_4$ and $[2^+]ClO_4$ were obtained by slow ether vapor diffusion into the corresponding acetonitrile solutions. Suitable crystals of appropriate dimensions were mounted on MiTeGen loops in random orientations. Preliminary examination and data collection were performed using a Bruker Kappa Apex-II Charge Coupled Device (CCD) detector system single crystal X-Ray diffractometer equipped with an Oxford Cryostream LT device. The data were collected using graphite monochromated Mo $K\alpha$ radiation ($\lambda = 0.71073$ Å) from a fine focus sealed tube X-ray source. Preliminary unit cell constants were determined with a set of 36 narrow frame scans. Typical data sets consist of a combination of ω and ϕ scan frames with a typical scan width of 0.5° and a counting time of 15–30 seconds per frame at a crystal to detector distance of ~ 4.0 cm. The collected frames were integrated using an orientation matrix determined from the narrow frame scans. Apex II and SAINT software packages³⁴ were used for data collection and data integration. The analysis of the integrated data did not show any decay. Final cell constants were determined by the global refinement of reflections from the complete data set. The data were corrected for systematic errors using SADABS³⁴ based on the Laue symmetry using equivalent reflections. Structure solutions and refinements were carried out using the SHELXTL-PLUS software package.³⁵ The structures were refined with full matrix least-squares refinement by minimizing $\sum w(F_o^2 - F_c^2)^2$. All non-hydrogen atoms were refined anisotropically to convergence. Typically, H atoms are added at the calculated positions in the final refinement cycles.

DFT and TD-DFT calculations

The density functional theory (DFT) calculations were performed with the program package Gaussian 09. Single point and geometry optimization calculations were performed using the B3LYP functional^{36,37} along with the Stevens CEP-31G(d) valence basis sets and effective core potentials were employed.^{38,39} The CEP-31G(d) valence basis set is valence

triple- ζ for palladium and double- ζ for main group elements, with an additional d polarization function for Cl. This functional/basis set combination has been shown previously to reproduce good experimental parameters of Pd complexes.^{40,41} Single point calculations were performed using the crystallographic coordinates for 1^+-6^+ , with solvent and counteranion molecules being excluded. The calculated ground state wavefunctions were investigated by analyzing the frontier molecular orbitals and the atomic contributions to the spin density. The atomic contributions to frontier molecular orbitals were calculated using the program Chemissian.⁴² TD-DFT calculations were employed to obtain the predicted absorption bands and their major contributions transitions. The calculated UV-vis spectra were generated using the program GaussSum,⁴³ with a full width at half maximum (FWHM) value of 3750 cm^{-1} .

Conflicts of interest

The authors declare no competing financial interest.

Acknowledgements

We thank the DOE Catalysis Science Program (DE-FG02-11ER16254) for support. S. V. P. thanks the Office of Undergraduate Research at Washington University for support.

References

- 1 A. Roodt, S. Otto and G. Steyl, *Coord. Chem. Rev.*, 2003, **245**, 121.
- 2 M. Akita and S. Hikichi, *Bull. Chem. Soc. Jpn.*, 2002, **75**, 1657.
- 3 W. E. Piers and D. J. H. Emslie, *Coord. Chem. Rev.*, 2002, **233–234**, 131.
- 4 S. P. Flanagan and P. J. Guiry, *J. Organomet. Chem.*, 2006, **691**, 2125.
- 5 A. Togni, N. Bieler, U. Burckhardt, C. Köllner, G. Pioda, R. Schneider and A. Schnyder, *Pure Appl. Chem.*, 1999, **71**, 1531.
- 6 R. C. J. Atkinson, V. C. Gibson and N. J. Long, *Chem. Soc. Rev.*, 2004, **33**, 313.
- 7 L. Cavallo, A. Correa, C. Costabile and H. Jacobsen, *J. Organomet. Chem.*, 2005, **690**, 5407.
- 8 E. A. B. Kantchev, C. J. O'Brien and M. G. Organ, *Angew. Chem., Int. Ed.*, 2007, **46**, 2768.
- 9 G. Helmchen and A. Pfaltz, *Acc. Chem. Res.*, 2000, **33**, 336.
- 10 G. B. Shul'pin, *Dalton Trans.*, 2013, **42**, 12794.
- 11 A. J. Canty, *Acc. Chem. Res.*, 1992, **25**, 83.
- 12 X. Chen, K. M. Engle, D.-H. Wang and J.-Q. Yu, *Angew. Chem., Int. Ed.*, 2009, **48**, 5094.
- 13 O. Daugulis, H.-Q. Do and D. Shabashov, *Acc. Chem. Res.*, 2009, **42**, 1074.
- 14 K. Muniz, *Angew. Chem., Int. Ed.*, 2009, **48**, 9412.
- 15 T. W. Lyons and M. S. Sanford, *Chem. Rev.*, 2010, **110**, 1147.
- 16 P. Sehnal, R. J. K. Taylor and I. J. S. Fairlamb, *Chem. Rev.*, 2010, **110**, 824.
- 17 D. C. Powers and T. Ritter, *Top. Organomet. Chem.*, 2011, **35**, 129.
- 18 L. M. Mirica and J. R. Khusnutdinova, *Coord. Chem. Rev.*, 2013, **257**, 299.
- 19 J. R. Khusnutdinova, N. P. Rath and L. M. Mirica, *J. Am. Chem. Soc.*, 2010, **132**, 7303.
- 20 J. R. Khusnutdinova, N. P. Rath and L. M. Mirica, *Angew. Chem., Int. Ed.*, 2011, **50**, 5532.
- 21 J. R. Khusnutdinova, N. P. Rath and L. M. Mirica, *J. Am. Chem. Soc.*, 2012, **134**, 2414.
- 22 J. R. Khusnutdinova and L. M. Mirica, in *C-H and C-X Bond Functionalization: Transition Metal Mediation*, ed. X. Ribas, Royal Society of Chemistry, 2013, p. 122.
- 23 J. Luo, J. R. Khusnutdinova, N. P. Rath and L. M. Mirica, *Chem. Commun.*, 2012, **48**, 1532.
- 24 J. Luo, N. P. Rath and L. M. Mirica, *Organometallics*, 2013, **31**, 3343.
- 25 J. R. Khusnutdinova, N. P. Rath and L. M. Mirica, *Inorg. Chem.*, 2014, **53**, 13112.
- 26 F. Tang, F. Qu, J. R. Khusnutdinova, N. P. Rath and L. M. Mirica, *Dalton Trans.*, 2012, **41**, 14046.
- 27 F. Tang, Y. Zhang, N. P. Rath and L. M. Mirica, *Organometallics*, 2012, **31**, 6690.
- 28 A.-L. Gassner, C. I. Duhot, J.-C. G. Bünzli and A.-S. Chauvin, *Inorg. Chem.*, 2008, **47**, 7802.
- 29 F. Bottino, M. Di Grazia, P. Finocchiaro, F. R. Fronczek, A. Mamo and S. Pappalardo, *J. Org. Chem.*, 1988, **53**, 3521.
- 30 See the ESI.†
- 31 Y. Si, Y. Liu, G. Gahungu, X. Qu and Z. Wu, *Mol. Phys.*, 2013, **111**, 3716.
- 32 D. F. Evans, *J. Chem. Soc.*, 1959, 2003.
- 33 G. A. Bain and J. F. Berry, *J. Chem. Educ.*, 2008, **85**, 532.
- 34 *Bruker Analytical X-Ray*, Madison, WI, 2008.
- 35 G. Sheldrick, *Acta Crystallogr., Sect. A: Found. Crystallogr.*, 2008, **64**, 112.
- 36 A. D. Becke, *J. Chem. Phys.*, 1993, **98**, 1372.
- 37 C. T. Lee, W. T. Yang and R. G. Parr, *Phys. Rev. B: Condens. Matter Mater. Phys.*, 1988, **37**, 785.
- 38 W. J. Stevens, H. Basch and M. Krauss, *J. Chem. Phys.*, 1984, **81**, 6026.
- 39 W. J. Stevens, M. Krauss, H. Basch and P. G. Jasien, *Can. J. Chem.*, 1992, **70**, 612.
- 40 N. A. Foley, M. Lail, J. P. Lee, T. B. Gunnoe, T. R. Cundari and J. L. Petersen, *J. Am. Chem. Soc.*, 2007, **129**, 6765.
- 41 A. S. Veige, L. M. Slaughter, P. T. Wolczanski, N. Matsunaga, S. A. Decker and T. R. Cundari, *J. Am. Chem. Soc.*, 2001, **123**, 6419.
- 42 L. Skripnikov, *Chemissian, version 1.771*, 2010, <http://www.chemissian.com>, accessed June 2016.
- 43 N. M. O'Boyle, A. L. Tenderholt and K. M. Langner, *J. Comput. Chem.*, 2008, **29**, 839.